



Static pressure-driven microfluidic gradient generator for long-term cell culture and adaptive cytoprotection analysis

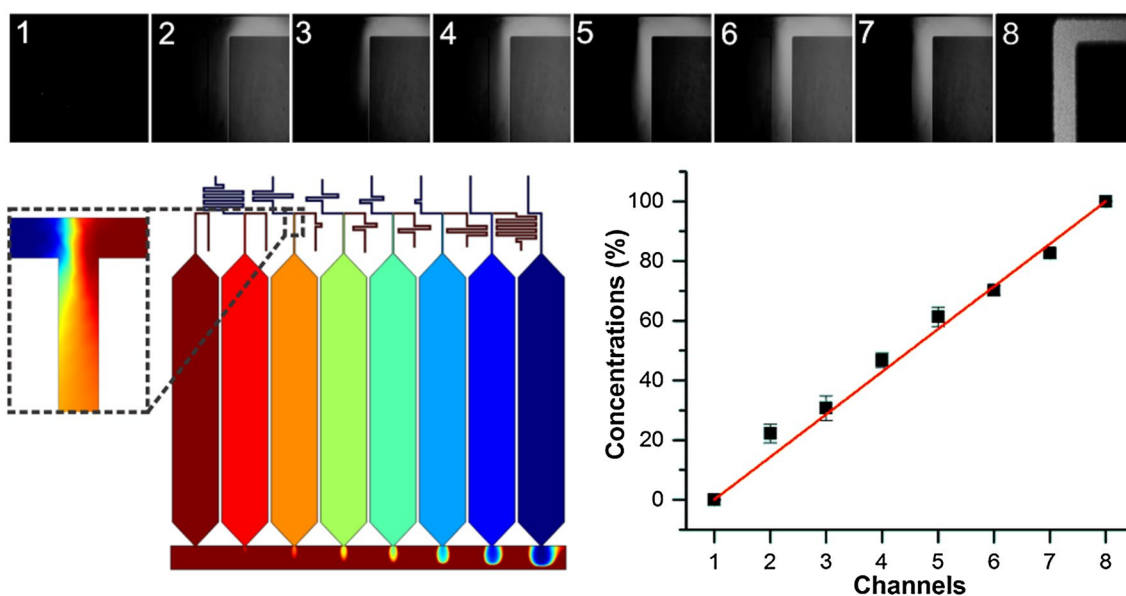
Xing Zhao¹ · Xinghua Yan¹ · Yiwei Li¹ · Bi-Feng Liu¹

Received: 24 August 2018 / Accepted: 21 March 2019 / Published online: 1 April 2019
© Springer-Verlag GmbH Germany, part of Springer Nature 2019

Abstract

Microfluidic gradient generators have largely benefitted high-throughput analysis of cellular responses, but are required to more precisely control culture parameters such as flow-induced shear stress. Here, a novel pump-free microfluidic gradient generator was proposed to generate a shear-free microenvironment for long-term cell culture and adaptive cytoprotection analysis. The microfluidic microchip was designed with a tunable network to generate pre-defined biochemical gradients. This device employed a static pressure to drive the flow at a low flow rate of 0.2 nL s^{-1} , which further benefited long-term cell culturing and stimulation by providing a shear-free ($7.1 \times 10^{-7} \text{ Pa}$) microenvironment. With the merits of pump free and shear free, this device was further used for the application used to analyze the adaptive cytoprotection behaviors of cells in response to reactive oxygen species. Our study showed that pretreatment of a sublethal dose of hydrogen peroxide significantly enhanced the tolerance of NIH 3T3 cells to lethal dose oxidative stress. Conclusively, the results confirmed that our novel microfluidic device was a highly efficient way to analyze adaptive cytoprotection behaviors of cells with advantages of high throughput, flexibility, stability, portable and low sample consumption, by providing shear-free and biochemistry well-defined cell microenvironments even without the requirement of external setups.

Graphical abstract



Xing Zhao and Xinghua Yan contributed equally to this work.

Extended author information available on the last page of the article

Keywords Microfluidics · Long-term cell culture · Cytoprotection · Single-cell analysis

1 Introduction

Microfluidic systems have been widely used in many areas including cell culturing, bio-detection and single-cell analysis (Morel et al. 2012; Li et al. 2015; Li et al. 2013; Li et al. 2014). A controlling microenvironment for cells is essential for understanding the complex dose-dependent effects that biochemicals have on cell growth, regeneration, and differentiation (Mehling and Tay 2014; Sackmann et al. 2014; Young and Beebe 2010). For the interest in illuminating these phenomena, first-generation biomolecule gradient platforms were developed including chambers and gel matrices based on the diffusion of the molecules (Boyden 1962; Brown 1982; Keller et al. 1977; Wilkinson and Lackie 1983; Zicha et al. 1991). However, these techniques have drawbacks in the spatiotemporal control and lack of quantitative characterization of these systems. To address this issue, serial dilution microfluidic devices were fully developed, which exploited the unique mass transfer phenomena presented at the microscale to precisely generate chemical gradients with pre-defined profiles and functions (Cimetta et al. 2010; Hosokawa et al. 2011; Selimovic et al. 2011). However, these techniques suffered for cell culture from the hydrodynamic shear stresses, which potentially damaged the cells. More recently, several types of microfluidic devices have emerged to address the limitations of the shear stress problem. Devices with high-resistance microchannels have been proposed with a significantly reduced shear stress without compromising the stability of the gradients (Atencia et al. 2009; Keenan et al. 2006; Li et al. 2007; Shamloo et al. 2008). Another type of device employed hydrogels (Morel et al. 2012; Abhyankar et al. 2008; Xu et al. 2013) or functionalized porous membranes (Abhyankar et al. 2006; Cate et al. 2010; de Jong et al. 2006; Kim et al. 2009) to separate the cultured cells and fluids, which provided cells a shear-free microenvironment (with cells on the other side of the membrane or hydrogel). However, the complex fabrication process impeded their widespread use. Thus, there is an urgent need for a technique that could generate stable shear-free biochemical gradients with easy operation and fabrication.

Herein, we presented a pump-free microfluidic gradient generator to provide a shear-free gradient microenvironment for long-term cell culture and stimulation. The dilution ratio of two stock solutions in this device was pre-defined according to the ratio of the lengths of the two distribution channels regardless of the flow rate and driven pressure. This design highly increased the stability of the formed gradients, especially under low flow rates though eliminating errors in solution injection. To minimize the shear force, a static

pressure was employed to drive the flow instead of conventional pumps and syringes. This design, without requirements of a syringe or pump, not only simplified the external setups but also eliminated the equipment errors. Due to the low flow rate, our device also largely reduced sample consumption as compared to the conventional microfluidic devices. More importantly, our device generated shear-free cell microenvironments with well-defined biochemistry for long-term cell culturing and stimulation. Both computational fluid dynamics (CFD) simulation and flow visualization experiment were carried out to validate the generated gradients. The flow rate of the individual microchannel was measured using the particle image velocimetry (PIV) method to be 0.2 nL s^{-1} . Shear stress was calculated to be $7.1 \times 10^{-7} \text{ Pa}$, which confirmed the cell-friendly shear-free microenvironment. To further validate, 5 days' culturing of NIH 3T3 cells only consumed $\sim 700 \mu\text{L}$ medium, while maintaining high cell viability.

Free radicals known as reactive oxygen species (ROS) randomly damage cellular constituents, including lipids, proteins, and DNA, which further influence a variety of disorders, diseases, cancer, and aging (Lee and Um 1999). One of the promising strategies to prevent damage is to induce adaptive cytoprotection of cells through presenting a physiologic non-toxic oxidative stimulant (Chen et al. 2005; de Almeida et al. 2008; Jang and Surh 2001; Sayin et al. 2012; Seo et al. 2004). To our knowledge, no report has been found on the use of a microfluidic chip for achieving a high-throughput adaptive cytoprotection analysis. Here, the pump-free microfluidic gradient generator was further used for application to adaptive cytoprotection analysis. After the cells were fully attached on the cell culture chamber, hydrogen peroxide solutions of various concentrations were generated automatically for the pretreatments. After precondition, cells were further challenged by a high dose of lethal hydrogen peroxide. Annexin-V/propidium iodide (PI) assay was performed to quantify cell apoptosis. Results indicated that the pretreatment of a low dose of hydrogen peroxide significantly protected NIH 3T3 cells against the cytotoxicity of a high dose of lethal hydrogen peroxide. Conclusively, this novel pump-free microfluidic gradient device generated a shear-free microenvironment with on-demand gradients, which provided a new strategy for high-throughput single-cell analysis including adaptive cytoprotection analysis.

2 Experiments

2.1 Design principle

The proposed gradient generator was based on the adjustment of volumetric flow rates of two liquids to get the pre-defined dilution ratio. A theory we established previously was employed to calculate the volumetric flow rates of two liquids at the two distribution channels (Table 1).

The equation for the design principle was carried out from the Hagen–Poiseuille equation. The equation we presented below shows the relationship that the expected concentration can be calculated from the ratio of the lengths of two distribution channels:

$$C_{\text{expected}} = \frac{Q_a \times C_a + Q_b \times C_b}{Q_a + Q_b} = \frac{L_a \times C_b + L_b \times C_a}{L_a + L_b}, \quad (1)$$

where C_{expected} represents the expected concentration; C_a and C_b represent the concentration of two stock solutions a and b respectively; L_a and L_b represent the lengths of the bifurcated channels for stock solution a and b , respectively; Q_a and Q_b the volumetric flow rates of laminar flows of two stock solutions a and b , respectively.

2.2 Materials and reagents

Chemicals such as CaCl_2 , NaOH , HEPES, NaCl , D-glucose , KH_2PO_4 , MgCl_2 , K_2HPO_4 , HCl , H_2O_2 , KCl , and fluorescein were purchased from Sinopharm Chemical Reagent (Shanghai, China). 488 Annexin-V/Dead Cell Apoptosis Kit with 488 Annexin-V and PI was purchased from Alexa Fluor (Carlsbad, CA). Tyrode’s solution was prepared freshly as the buffer solution containing CaCl_2 , 1.3 mM; MgCl_2 , 1 mM; D-glucose , 10 mM; NaCl , 137 mM; KCl , 5.4 mM; and HEPES, 10 mM (pH 7.2), which was filtered through a 0.22 μm porous membrane for sterilization. Fluorescein was prepared in the buffer solution at a final concentration of 20 μM for flow visualization experiments. Annexin-V was prepared in the Tyrode’s solution at a final concentration of 15 $\mu\text{L mL}^{-1}$ and PI was prepared in the buffer solution at a concentration of 5 $\mu\text{g mL}^{-1}$.

2.3 Cell culture

NIH 3T3 cells were cultured using culture flasks (BD Falcon) containing 5 mL Dulbecco’s Modified Eagle Medium (DMEM) medium with 10% (v/v) fetal bovine serum. Cells

were cultured (5% CO_2 , 90% humidified) at 37 °C using an incubator (Innova-Co 170; New Brunswick Scientific, UK) before use. To maintain cells in the exponential growth phase, NIH 3T3 cells were subcultured at a ratio of 1:3 every 3 days. A 3 min treatment of 0.25% (w/v) Trypsin–EDTA solution (Gibco) was performed to detach cells from the flask for harvest.

2.4 Microfabrication

The mold was fabricated with SU-8 1070 (Gersteltec Sarl, Switzerland) on a silicon wafer n type <100> using the standard soft-lithography technique. The polydimethylsiloxane (PDMS) layer was fabricated by rapid prototyping according to the SU-8 mold using a PDMS mixture of monomer and curing agent (Sylgard 184, Dow Corning, USA) with a ratio of 10:1 (wt/wt). After the PDMS layer was peeled off the mold, the inlets were fabricated using a hole puncher. The PDMS layer, glass slide and reservoir ports were then irreversibly bonded together after the treatment of oxygen plasma to assemble the final chip (shown in Fig. 1a). The height of the channels was designed to be 25 microns. The width of all the channels for mixing and distributing liquids was designed to be 200 microns, while the width of the cell culturing chamber was 5.85 mm to allow enough space for long-term cell growth.

2.5 Operation procedures

No syringe or pump was employed for this passive microfluidic gradient generator. Prior to each use, two stock solutions should be added to the reservoir ports and the liquid levels of stock solutions should be carefully adjusted so that they are equal. Liquids would flow into the channels under the static stress, and further be merged to generate gradients according to the ratio of the lengths of the distribution channels (shown in Fig. 1b).

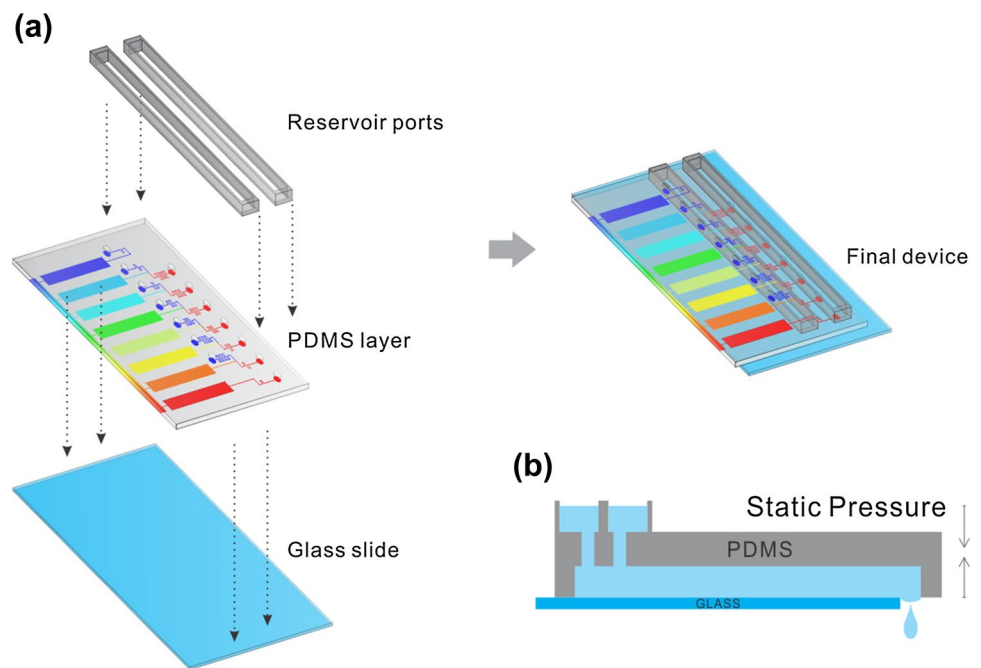
2.6 Optical imaging system and the measurement of fluorescence

An inverted fluorescence microscope (IX71, Olympus, Japan) with a charge-coupled device (CCD) camera (Evolve 512, photometrics, USA) was employed for our experiments. A 10 \times objective lens (N.A. 0.3) with a filter cube of U-MWIB2 (460–490 nm band-pass filter, 505 nm diachronic mirror, 510 nm high-pass filter, Olympus, Japan) was used to monitor the flow visualization experiments. The cubes of U-MWG2

Table 1 The length of the distribution channels with the linear concentration design

Channels	1	2	3	4	5	6	7	8
Channel of 0% stock solution	840 (μm)	5880	2940	1960	1470	1176	980	0
Channel of 100% stock solution	0	980	1176	1470	1960	2940	5880	840

Fig. 1 Schematics of the pump-free microfluidic gradient generator assembly (a) and section view (b)



(510–550 nm band-pass filter, 570 nm diachronic mirror, 590 nm high-pass filter, Olympus, Japan) and U-MWIB2 (460–490 nm band-pass filter, 505 nm diachronic mirror, 510 nm high-pass filter, Olympus, Japan) were used for the apoptosis assay using Annexin-V and PI.

2.7 CFD simulation

To evaluate the structure of the pump-free microfluidic gradient generator, numerical simulation was carried out using comsol. A finite volume model was employed to validate the dilution efficiency. The adopted simulation procedure was similar to our previous work (Chen et al. 2013). The liquids in inlets were set as 0 and 1 in concentration, 10^3 kg m^{-3} in density, 10^{-3} Pa s in viscosity and $4.9 \times 10^{-10} \text{ m}^2 \text{ s}^{-1}$ in diffusion coefficient. The distribution of the liquid was obtained by solving the continuity equation, Navier–Stokes equation and diffusion–convection equation until the increment in each variable fell below 1×10^{-5} .

3 Results and discussion

3.1 Numerical simulation of gradient generation

Numerical simulations were applied to validate the feasibility of the pump-free microfluidic gradient generator, which provided guidance for further experiments. The numerical simulation was carried out by COMSOL multiphysics TM (COMSOL 3.4, Sweden). The flow patterns and solution exchanges of the samples were characterized and calculated

by the incompressible Navier–Stokes equation. To demonstrate the dilution ratio of different channels, a dilute solution (water) and a stock solution of fluorescein (100%) were used as the materials. The flow pressure was set as 19.6 Pa, which was calculated from the atmosphere pressure, the cross-section areas of the inlets and outlets, and the liquid level differences.

At an equivalent pressure of 19.6 Pa, the dilution result of two stock solutions (water and 100% fluorescein solution) was shown in Fig. 2. In the cell culturing chambers, the chemical concentrations gradually increased from right to left according to the relative lengths of the distribution channels, in which colors from blue to red represented the relative concentrations. The mixing efficient was also validated in this numerical study. The two liquids began to mix when they met at the confluent points. The mixing was completed in a short distance as indicated by the merged interface. The average intensities in a cross-section area of the channels at the downstream of the mixing channels were calculated to validate the well-defined gradient profile. As seen in the results shown in Fig. 2b, the correlation coefficient of linear regression, R^2 , was higher than 0.99. The numerical simulation results indicated that the pump-free microfluidic device was able to generate a well-defined concentration profile accurately.

The numerical study was also used to validate the flow rate (Fig. 2b). The small flow rate ensured the ultralow shear force according to Eq. (2) (Sun et al. 2011; Batchelor and Batchelor 1967; Levitan et al. 2000):

$$\tau = \frac{6\eta Q}{wh^2}, \quad (2)$$

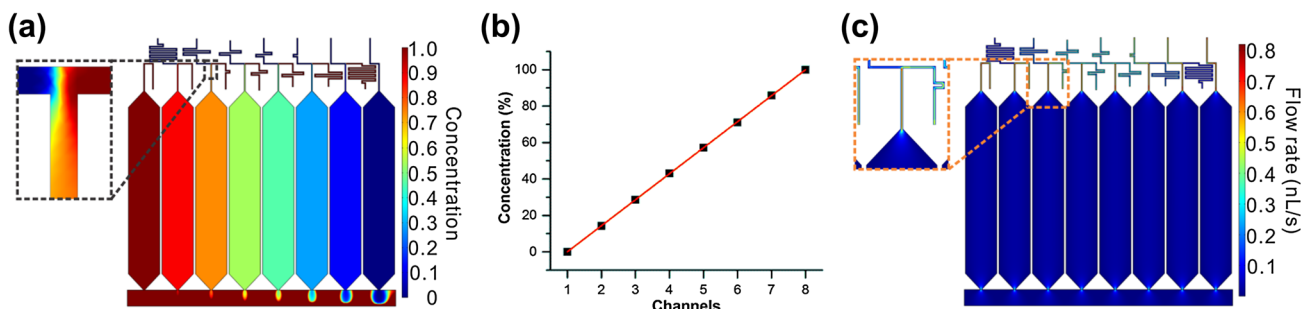


Fig. 2 Results of numerical simulation. **a** Visible CFD study results of linear gradient concentration. **b** Quantitative analysis of the gradient concentrations in numerical simulation. **c** Visible results of flow rates in the CFD study of linear gradient dilution

where τ represents the average shear stress on the cells, η represents the viscosity of the fluid, Q represents the flow rate, h represents the height of the channel and w is the width of the microchannel. For the numerical simulation, a shear stress value of $\sim 1 \times 10^{-6}$ Pa in this pump-free device is safe for cell culture.

3.2 Flow visualization experiment

To further validate the biochemical gradients formed in the pump-free microfluidic device, a flow visualization experiment was further performed on chips using fluorescein. After the fluorescein solution and buffer solution were loaded into the reservoir ports, respectively, the liquids would flow into the channels automatically due to the static pressures. Two liquids merged at the confluent points, and then were mixed to generate the expected concentrations. The diffusion of the fluorescein was observed at the downstream of the confluent point. As shown in Fig. 3a and c, at the confluent points, the width of the fluorescein solution increased from channel 1 to channel 8. The average fluorescent intensities were calculated in a cross-section area of the channels, which also increased as the width of the fluorescein solution.

Our results were presented as a ratio of the final fluorescence intensity to the initial fluorescence intensity (100% stock solution). The quantitative analysis of our results (shown in Fig. 3b) was consistent with the theoretical design and the CFD simulation results. A well-defined concentration profile was precisely generated according to the design of microfluidic device regardless of the flow pressure. The correlation coefficient of the linear regression, R^2 , for the linear regression was higher than 0.99. In comparison to diffusion-based gradient generators and serial dilution microfluidic devices, the static pressure-driven device provided a more stable and precise biochemical gradient by eliminating the error caused by the syringes and pumps employed. We also quantified the flow rates in our chip by either tracking fluorescent microparticles or calculating from the expelled liquids. The two results were consistent with each other, which indicated a flow rate of 0.2 nL s^{-1} , as

well as a total medium consumption of 1 mL for 1-week long-term culturing. Then, the corresponding shear stress was calculated to be 7.1×10^{-7} Pa from the measured flow rate, which was not harmful to the living cells according to the previous paper (Sun et al. 2011).

3.3 Performance of the mixing

The two laminar flows that merged at the confluent point should be completely mixed to generate a well-defined concentration. The principle of mixing in the pump-free microfluidic gradient generator was based on molecular diffusion. Particularly, the mixing was usually unstable, dependent and affected by the flow conditions such as flow rates and liquid viscosity. To address this issue, long mixing channel or some embedded mixers were usually employed, which unexpectedly increased the complexity and redundancy of the structures. In this paper, the mixing benefited from the low flow rates driven by the static pressure. As indicated by the diffusive mixing equation (Kamholz and Yager 2001; Veenstra et al. 1999; Ismagilov et al. 2000):

$$t_{\text{mix}} = w_f^2 / \pi^2 D, \tag{3}$$

where t_{mix} represents the required time for complete mixing, w_f represents the diffuse distance, D represents the diffusion coefficient of solute molecular.

The uniformity of the fluorescein concentration in the microchannels after mixing was examined. σ was carried out to quantify the mixing efficiency, which was defined as a measure of homogeneity of the solution. The equation was based on the standard deviation of the pixel intensity and the average intensity in a line across the channels presented here:

$$\sigma = 1 - \frac{\sqrt{\frac{1}{n} \sum_{i=1}^n (I_i - \langle I \rangle)^2}}{\langle I \rangle}, \tag{4}$$

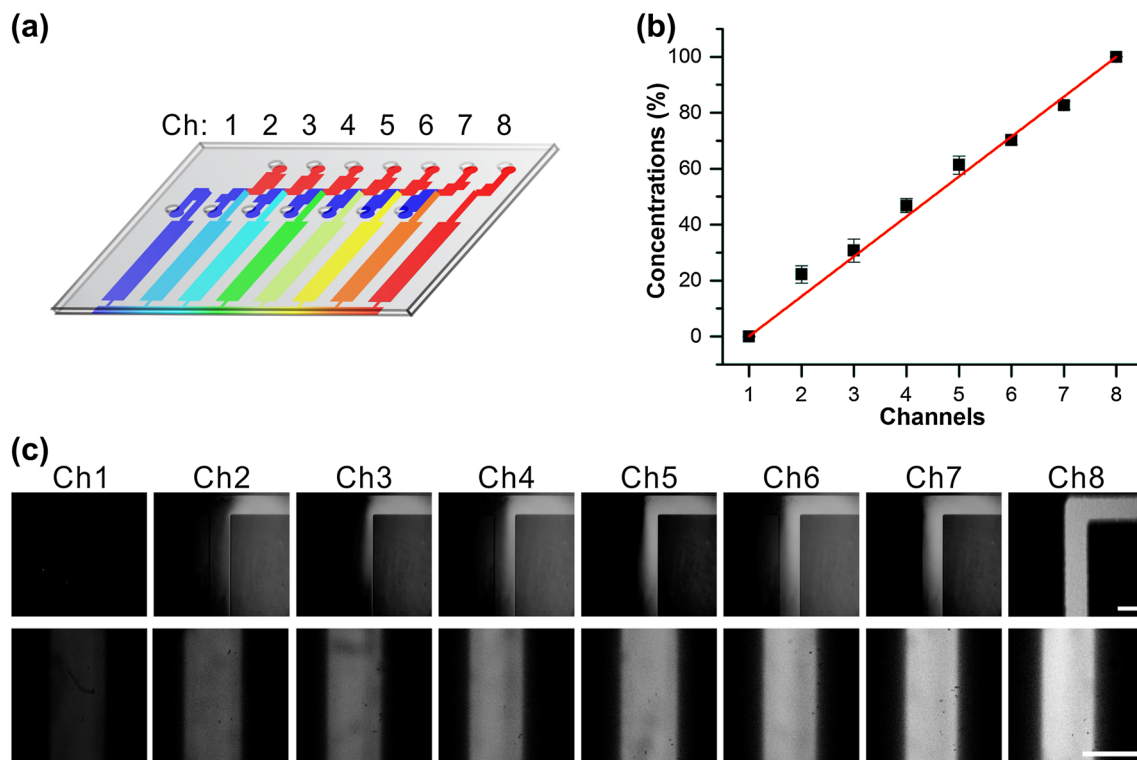


Fig. 3 Results of flow visualization experiments. **a** Schematic illustration of the chip and the corresponding channels. **b** Quantitative analysis of the gradient concentrations in numerical simulation. **c**

Images of the dilution ratio of the two liquids merged at eight parallel confluent microchannels. Scale bar, 200 μm

where I_i is the background-corrected value of the i th pixel, $\langle I \rangle$ is the average value of the background-corrected intensity, and n is the pixel number in the selected area. The distribution of intensities in a completely mixed solution should have an σ value of 1. However, the system noise practically resulted in a nonzero σ even for completely mixed solutions.

As shown in Fig. 4b, mixing in this device with various liquid height differences was examined. The varied liquid height differences led to varied driven static pressures. Mixings with liquid height difference ranges from 2 to 10 mm was examined (H1: 2 mm, H2: 4 mm, H3: 6 mm, H4: 8 mm, H5: 10 mm). The mixing ratio of two distributed solutions was 1:1. The σ was above 0.8 for all, while the σ with H1 and H2 were above 0.9. This result reveals that a liquid level larger than 4 mm could ensure complete mixing. σ was also calculated in all eight channels. σ was above 0.9 for all from channel 1 to channel 8, which indicated that liquids in all eight channels were fully mixed at the position of the cross-line, as shown in Fig. 4c.

The width of the confluence channels remained the same in the design. The diffuse distance w_f ranged from 1/8 to 7/8 of the channel width. Thus, t_{mix} in this device was maximum when the w_f was either 1/8 or 7/8. The flow rates determined the length of the channels required for complete mix. In the

widely used pump-driven microfluidics, a long mixing channel is required to achieve complete mixing. In this pump-free microfluidic device, the low flow rate ensured complete mixing in a very short distance. The numerical study result shown in Fig. 2c indicated the short mixing distance. Mixing results in flow visualization experiment shown in Fig. 4a were consistent with the numerical study. Two stock liquids in this device could be completely mixed in a short length. The critical length of channel required for complete mixing was evaluated by measuring the homogeneity of the solution along the length from the confluent point. The place, where the homogeneity of the solution reached 90%, was defined as the critical point. The length between the confluent point and the critical point was defined by the critical length, and the critical length was measured to be 626 μm (Fig. 4d). Z-stack 3D image in the downstream was further reconstructed to show the complete mixing (Fig. 4e).

3.4 Long-term cell culture

The growth rate of NIH 3T3 cells was first demonstrated in the microfluidic device. Cells were seeded in eight culture chambers with a density of 3.4×10^5 cells ml^{-1} . The growth of NIH 3T3 cells was analyzed over 5 days. The average doubling time measured in these experiments was

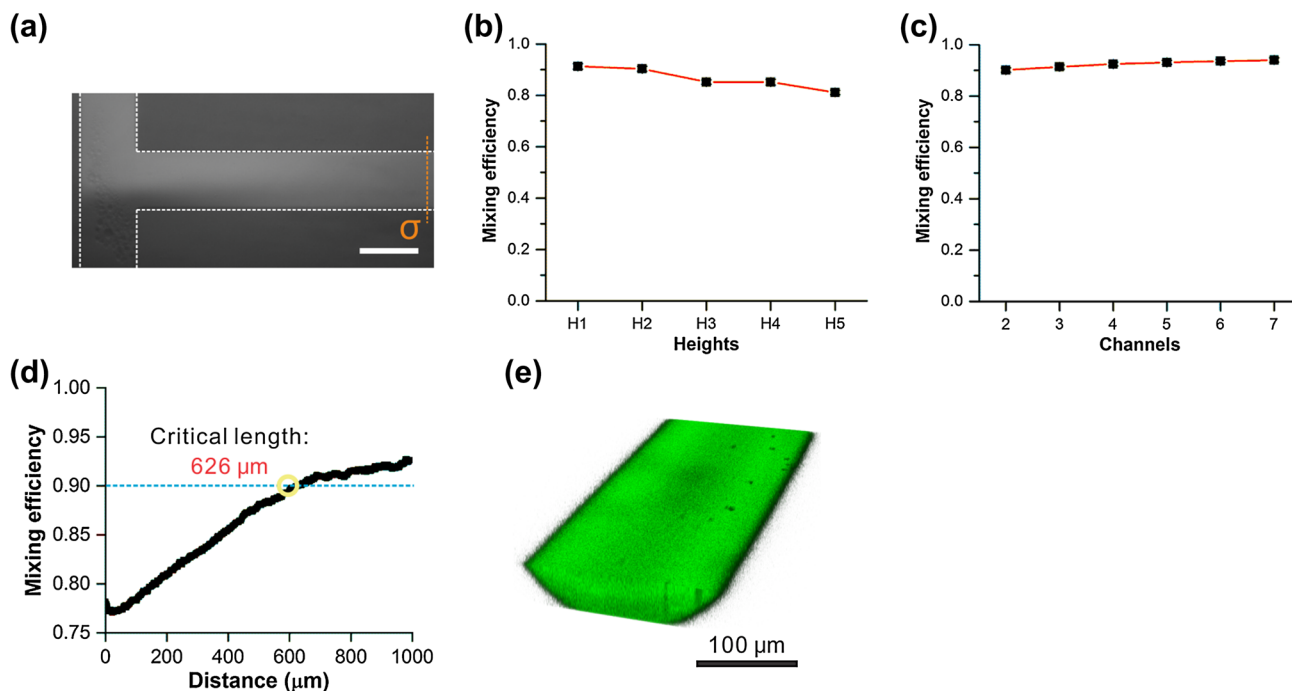


Fig. 4 Performance of the diffusion-based mixing. **a** Fluorescence image of the diffusion-based mixing. Mixing was completed in a short distance. Scale bar, 200 μm. **b** Quantitative analysis of mixing efficiency indicated at the orange line in **a** with different liquid level differences. **c** Quantitative analysis of mixing efficiency in eight chan-

nels. **d** Measurement of the mixing efficiency along the channel from the mixing initial point. The required length of the channel where the mixing efficiency reaches 0.9 was defined as the critical length. **e** z-stack 3D confocal image showed complete mixing (color figure online)

21.3 ± 0.5 h. Cell culture chamber was designed as 5.85 mm in width and 31 mm in length. Figure 5a showed an image of the cell chamber after the cell was fully set. The cells approached confluence on the 5th day. To validate the capability of this device for long-term cell culture, cell numbers in the chamber were calculated every day. As indicated by

the results shown in Fig. 5g, the cell number increased significantly during 5 days of culturing. The curve reflected a linear growth phase until the cells reached confluence followed by a stationary phase. Sequential live/dead assay was further carried out to examine cell viability in the pump-free microfluidic gradient generator. As a result, most of the cells

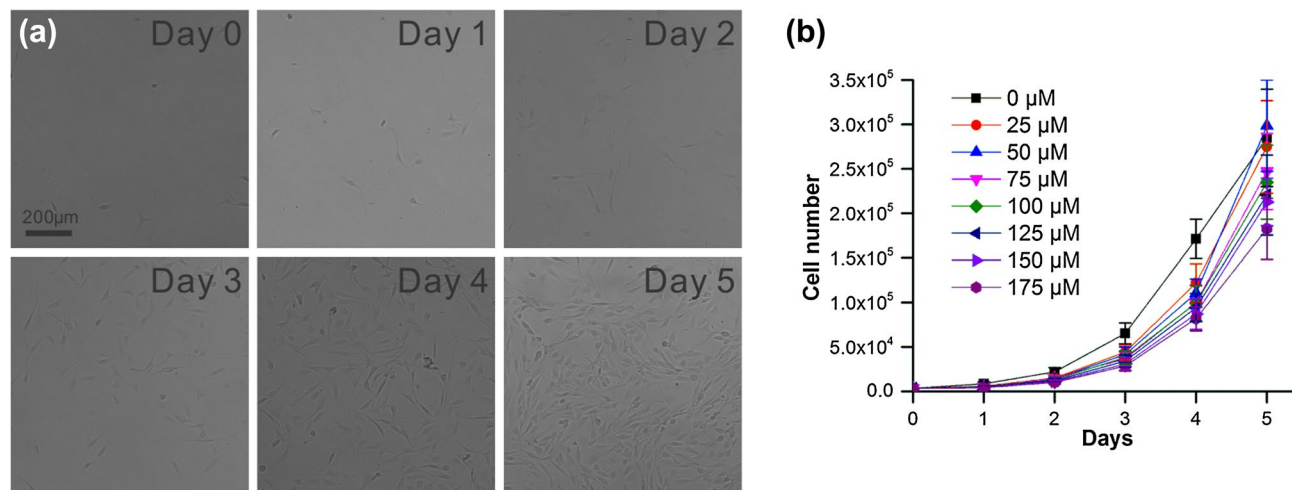


Fig. 5 Long-term cell culturing. **a** Images of cells grown in the chips in 5 days. Scale bar, 200 μm. **b** Growth curves of cells over 5 days of culturing. Cells were pretreated with hydrogen peroxide of various concentrations ranging from 0 to 175 μm

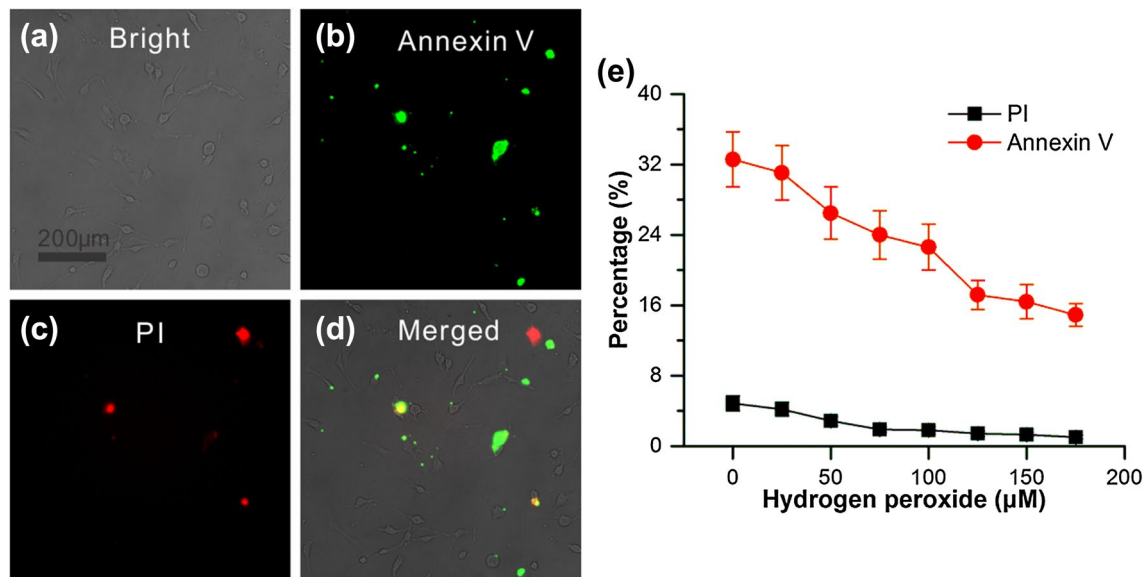


Fig. 6 Adaptive cytoprotection analysis. **a** Bright-field image of cells challenged with lethal hydrogen peroxide. **b** Fluorescence image of cells stained by Annexin V-FITC after lethal hydrogen peroxide treatment. **c** Fluorescence image of cells stained by PI after lethal hydro-

gen peroxide treatment. **d** Overlap image of challenged cells. **e** Quantitative analysis of adaptive cytoprotection. Cells were pretreated with hydrogen peroxide of various concentrations ranging from 0 to 175 μM

are viable (more than 95%). All the evidences indicated that the passive microfluidic gradient generator serves as a platform to perform long-term cell culture.

We simultaneously examined cells' response to the pretreatments of hydrogen peroxide of different concentrations in the same device. After cells were fully set in the cell culture chamber, cells were pretreated with hydrogen peroxide of various concentrations in this chip (varied from 25 to 175 μM). Growth curves were conducted by measuring the cell numbers. Cells treated with hydrogen peroxide exhibited a lag phase in growth in the first 2 days. The results shown in Fig. 5b indicated that hydrogen peroxide causes a transient growth arrest.

3.5 Adaptive cytoprotection analysis

Oxidative stress might cause damage of lipids, proteins, and DNA, which is involved in a variety of disorders, diseases, cancer, and aging. Thus, protection from oxidative insult has received much attention. Adaptive cytoprotection, caused by a physiologic nontoxic oxidative stimulant, was considered as a promising approach to enhance the tolerance of cells to oxidative stress. It is widely accepted that two major pathways of intracellular hydrogen peroxide detoxification—cellular catalase and glutathione peroxidase (GPx)—are activated and might be responsible for such adaptive cytoprotection.

Herein, the adaptive cytoprotection to hydrogen peroxide and the resulting protective effect against oxidative stress

have been analyzed using NIH 3T3 cells. After the cells were cultured in the microchamber for 24 h, hydrogen peroxide solutions of low concentrations were used to precondition cells for 24 h. After pretreatment with a low dose of hydrogen peroxide (ranged from 25 to 175 μM), cells were challenged by lethal hydrogen peroxide (500 μM) for 6 h. Annexin-V/propidium iodide assay was carried out to validate the induced apoptosis of NIH 3T3 cells. The cells challenged by lethal hydrogen peroxide are shown in Fig. 6a–d. As shown in Fig. 6e, direct exposure to lethal dose 500 μM hydrogen peroxide results in 27.72% of cells going through apoptosis. Nonetheless, pretreatment with hydrogen peroxide for 24 h prior to lethal hydrogen peroxide exposure arrested the apoptosis in a dose-dependent manner. The ratio of apoptosis decreased to 26.8% with 25 μM hydrogen peroxide pretreatment, which further decreased to 22.08% with 75 μM hydrogen peroxide pretreatment. A pretreatment with 175 μM hydrogen peroxide could further reduce the apoptosis ratio to 13.87% (Fig. 6e). Conclusively, pretreatment of sublethal doses of hydrogen peroxide significantly protected NIH 3T3 against the cytotoxicity induced by lethal hydrogen peroxide.

4 Conclusions

A pump-free and shear-free microfluidic gradient generator was proposed in this paper. The chip was designed to generate arbitrary gradients for specific biological studies.

This device simplified the structure of the multi-step divider serial dilution chip and provided more stability than the diffusion devices. Instead of syringes and pumps used in previous devices, static pressure was employed in our system for flow driven. With an extremely small but stable static pressure, gradient dilutions were generated with low flow rate. As indicted by numerical simulation and flow rate measurements, low flow rates ensured the shear-free cell microenvironment, which provided this method with a new strategy for long-term cell culture and stimulation. The device is easily fabricated and simply operational. No external equipment is required in this system, and this makes it a widely applicable tool in most biological labs and even portable. Finally, this study is the first one to report on the application of microfluidics to cell-based high-throughput adaptive cytoprotection analysis. Results showed that pretreatment of a low dose of hydrogen peroxide significantly protected NIH 3T3 cells against the cytotoxicity induced by reactive oxygen species. To sum up, pump-free microfluidic gradient chip generated an arbitrary well-defined gradient profile with stability and ultralow shear property, which provided a new strategy for long-term cell culture and could be further used for the application to adaptive cytoprotection analysis.

Acknowledgements The authors gratefully acknowledge the financial supports from National Natural Science Foundation of China (21475049, 31471257, 41430860 and 21275060) and National Key R&D Program of China (2016YFF0100801).


References

- Abhyankar VV, Lokuta MA, Huttenlocher A, Beebe DJ (2006) Characterization of a membrane-based gradient generator for use in cell-signaling studies. *Lab Chip* 6(3):389–393
- Abhyankar VV, Toepke MW, Cortesio CL, Lokuta MA, Huttenlocher A, Beebe DJ (2008) A platform for assessing chemotactic migration within a spatiotemporally defined 3D microenvironment. *Lab Chip* 8(9):1507–1515
- Atencia J, Morrow J, Locascio LE (2009) The microfluidic palette: a diffusive gradient generator with spatiotemporal control. *Lab Chip* 9(18):2707–2714
- Batchelor CK, Batchelor GK (1967) An introduction to fluid dynamics. Cambridge University Press, Cambridge
- Boyden S (1962) The chemotactic effect of mixtures of antibody and antigen on polymorphonuclear leucocytes. *J Exp Med* 115:453–466
- Brown AF (1982) Neutrophil granulocytes: adhesion and locomotion on collagen substrata and in collagen matrices. *J Cell Sci* 58:455–467
- Cate DM, Sip CG, Folch A (2010) A microfluidic platform for generation of sharp gradients in open-access culture. *Biomicrofluidics* 4(4):44105
- Chen ZH, Yoshida Y, Saito Y, Niki E (2005) Adaptation to hydrogen peroxide enhances PC12 cell tolerance against oxidative damage. *Neurosci Lett* 383(3):256–259
- Chen P, Chen P, Feng XJ, Du W, Liu BF (2013) Analysis of intercellular communication by flexible hydrodynamic gating on a microfluidic chip. *Anal Bioanal Chem* 405(1):307–314
- Cimetta E, Cannizzaro C, James R, Biechele T, Moon RT, Elvassore N, Vunjak-Novakovic G (2010) Microfluidic device generating stable concentration gradients for long term cell culture: application to Wnt3a regulation of β -catenin signaling. *Lab Chip* 10(23):3277–3283
- de Almeida LMV, Pineiro CC, Leite MC, Brolese G, Leal RB, Gottfried C, Goncalves CA (2008) Protective effects of resveratrol on hydrogen peroxide induced toxicity in primary cortical astrocyte cultures. *Neurochem Res* 33(1):8–15
- de Jong J, Lammertink RGH, Wessling M (2006) Membranes and microfluidics: a review. *Lab Chip* 6(9):1125–1139
- Hosokawa M, Hayashi T, Mori T, Yoshino T, Nakasono S, Matsunaga T (2011) Microfluidic device with chemical gradient for single-cell cytotoxicity assays. *Anal Chem* 83(10):3648–3654
- Ismagilov RF, Stroock AD, Kenis PJA et al (2000) Experimental and theoretical scaling laws for transverse diffusive broadening in two-phase laminar flows in microchannels. *Appl Phys Lett* 76(17):2376–2378
- Jang JH, Surh YJ (2001) Protective effects of resveratrol on hydrogen peroxide-induced apoptosis in rat pheochromocytoma (PC12) cells. *Mutat Res Genet Toxicol Environ Mutagen* 496(1–2):181–190
- Kamholz AE, Yager P (2001) Theoretical analysis of molecular diffusion in pressure-driven laminar flow in microfluidic channels. *Biophys J* 80(1):155–160
- Keenan TM, Hsu CH, Folch A (2006) Microfluidic “jets” for generating steady-state gradients of soluble molecules on open surfaces. *Appl Phys Lett* 89(11):114103. <https://doi.org/10.1063/1.2345914>
- Keller HU, Wilkinson PC, Abercrombie M, Becker EL, Hirsch JG, Miller ME, Ramsey WS, Zigmund SH (1977) A proposal for the definition of terms related to locomotion of leucocytes and other cells. *Cell Biol Int Rep* 1(5):391–397
- Kim T, Pinelis M, Maharbiz MM (2009) Generating steep, shear-free gradients of small molecules for cell culture. *Biomed Microdevices* 11(1):65–73
- Lee BR, Um HD (1999) Hydrogen peroxide suppresses U937 cell death by two different mechanisms depending on its concentration. *Exp Cell Res* 248(2):430–438
- Levitani I, Helmke BP, Davis PF (2000) A chamber to permit invasive manipulation of adherent cells in laminar flow with minimal disturbance of the flow field. *Ann Biomed Eng* 28(10):1184–1193
- Li CW, Chen RS, Yang MS (2007) Generation of linear and non-linear concentration gradients along microfluidic channel by microtunnel controlled stepwise addition of sample solution. *Lab Chip* 7(10):1371–1373
- Li YW, Feng XJ, Du W, Li Y, Liu BF (2013) Ultrahigh-throughput approach for analyzing single-cell genomic damage with an agarose-based microfluidic comet array. *Anal Chem* 85(8):4066–4073
- Li YW, Yan XH, Feng XJ, Wang J, Du W, Wang YC, Chen P, Xiong L, Liu BF (2014) Agarose-based microfluidic device for point-of-care concentration and detection of pathogen. *Anal Chem* 86:10653–10659. <https://doi.org/10.1021/ac5026623>
- Li Y, Feng X, Wang Y, Du W, Chen P, Liu C, Liu BF (2015) Assembly of multiple cell gradients directed by three-dimensional microfluidic channels. *Lab Chip* 15(15):3203–3210
- Mehling M, Tay S (2014) Microfluidic cell culture. *Curr Opin. Biotechnol* 25:95–102
- Morel M, Galas JC, Dahan M, Studer V (2012) Concentration landscape generators for shear free dynamic chemical stimulation. *Lab Chip* 12(7):1340–1346
- Sackmann EK, Fulton AL, Beebe DJ (2014) The present and future role of microfluidics in biomedical research. *Nature* 507(7491):181–189
- Sayin O, Arslan N, Guner G (2012) The protective effects of resveratrol on human coronary artery endothelial cell damage induced by hydrogen peroxide in vitro. *Acta Clin Croat* 51(2):227–235

- Selimovic S, Sim WY, Kirn SB, Jang YH, Lee WG, Khabiry M, Bae H, Jambovane S, Hong JW, Khademhosseini A (2011) Generating nonlinear concentration gradients in microfluidic devices for cell studies. *Anal Chem* 83(6):2020–2028
- Seo YJ, Lee JW, Lee EH, Lee HK, Kim HW, Kim YH (2004) Role of glutathione in the adaptive tolerance to H₂O₂. *Free Radic Biol Med* 37(8):1272–1281
- Shamloo A, Ma N, Poo MM, Sohn LL, Heilshorn SC (2008) Endothelial cell polarization and chemotaxis in a microfluidic device. *Lab Chip* 8(8):1292–1299
- Sun J, Chen P, Feng XJ, Du W, Liu BF (2011) Development of a microfluidic cell-based biosensor integrating a millisecond chemical pulse generator. *Biosens Bioelectron* 26(8):3413–3419
- Veenstra TT, Lammerink TSJ, Elwenspoek MC (1999) Characterization method for a new diffusion mixer applicable in micro flow injection analysis systems. *J Micromech Microeng* 9(2):199
- Wilkinson PC, Lackie JM (1983) The influence of contact guidance on chemotaxis of human neutrophil leukocytes. *Exp Cell Res* 145(2):255–264
- Xu BY, Hu SW, Qian GS, Xu JJ, Chen HY (2013) A novel microfluidic platform with stable concentration gradient for on chip cell culture and screening assays. *Lab Chip* 13(18):3714–3720
- Young EWK, Beebe DJ (2010) Fundamentals of microfluidic cell culture in controlled microenvironments. *Chem Soc Rev* 39(3):1036–1048
- Zicha D, Dunn GA, Brown AF (1991) Analyzing chemotaxis using the Dunn direct-viewing chamber. *J Cell Sci* 99(Pt 4):769–775

Publisher's Note Springer Nature remains neutral with regard to jurisdictional claims in published maps and institutional affiliations.

Affiliations

Xing Zhao¹ · Xinghua Yan¹ · Yiwei Li¹  · Bi-Feng Liu¹

✉ Yiwei Li
liberatark@gmail.com

Science and Technology, Huazhong University of Science and Technology, Wuhan 430074, China

¹ The Key Laboratory for Biomedical Photonics of MOE at Wuhan National Laboratory for Optoelectronics-Hubei Bioinformatics and Molecular Imaging Key Laboratory, Department of Biomedical Engineering, College of Life